Three Stages of Crystallization in Poly(ethylene terephthalate) during Mass Transport

Hao Ouyang,*,† Wen-Hao Lee,† and Ming-Chih Shih‡

Department of Materials Engineering and Department of Physics, National Chung Hsing University, 250, Kuo Kuang Rd., Taichung 402, Taiwan, R.O.C.

Received June 3, 2002; Revised Manuscript Received August 3, 2002

ABSTRACT: The mass transport and the evolution of related phase transformation in poly(ethylene terephthalate) (PET) were studied. Solvent-induced crystallization, which occurs during the transport process in PET, is mainly explained as the result of plasticization. The degree of plasticization depends on the concentration of solvent. Therefore, the behavior of crystallization can be closely related to the mechanism of mass transport. The evolution of transformation was studied by small-angle X-ray scattering (SAXS), Fourier transform infrared (FTIR) spectroscopy, optical microscopy (OM), and the density gradient column. During the process of transport, the Fickian mechanism dominated during the first stage of crystallization, and swelling was found to be responsible for the occurrence of most crystallization in the second stage. The first two processes can be classified as the "primary crystallization". The last stage is associated with the "secondary crystallization".

Introduction

Introduction of an interactive organic solvent with low molecular weight can induce crystallization in the glassy poly(ethylene terephthalate) (PET) by plasticizing the material. The enough soluble acetone in amorphous PET will depress the glass transition temperature below the environmental temperature and helps the chains inside the polymer overcome the activation barrier to attain the more stable state. Kinetically, these long chains will be with sufficient mobility to rearrange themselves into more stable configuration: the crystalline state in this study. Therefore, the existence of critical concentration of diluent necessary for the solvent-induced crystallization is expected.[1] If the rate of crystallization surpasses the rate of penetrant transport into the sample, then the overall crystallization is transport limited and vice versa. Since the concentration of solvent inside the PET has a great influence on the degree of plasticization and therefore the associated induced crystallization, it is necessary to describe the mass-transport mechanisms in the beginning. The mass transport of organic solvents in the glassy polymer has been classified by Alfrey et al.[2] to include case I (Fickian) and case II (swelling mechanisms). Anomalous diffusion is a mixture of case I and case II. When the kinetics is dominated by case I, the sorption is proportional to the square root of time, $t^{1/2}$, whereas the mass uptake is proportional to t for the prevalence of case II. Kwei et al.[3−6] proposed a mathematical model to describe case I and case II transport phenomena in the finite and semiinfinite mediums. Perterlin also presented a model of case II advancing front preceded by a Fickian foot.[7] Harmon et al.[8,9] investigated the transport of methanol in a deformed, cross-linked poly(methyl methacrylate) (PMMA) using a modified Kwei's equation. Durning et al.[1,10−12] incorporated the influence of crystallization in the behavior of mass transport, and the transport phenomenon turns out to be much more complicated. The aspect ratio of the specimen shape can further influence the analysis of transport and related crystallization because of the effect of the degree of dimension on the diffusion.[1,13,14] It is well-known that the case I mechanism is related to the concentration gradient, and the case II model is associated with the stress relaxation. If the swelling prevails during solvent-induced crystallization, there are significant stresses and related strains built up in the matrix. This has been confirmed in our former work.[15] This kind of large stress relaxation is usually not observed during the thermal crystallization. Therefore, it is interesting to study the relationship between the transport mechanism and corresponding solvent-induced crystallization.

Experimental Section

This work involves experimental studies of acetone absorption, small-angle X-ray scattering (SAXS), Fourier transform infrared (FTIR) spectroscopy, density gradient column, and optical microscopy. The amorphous PET (ES301465) sheet was purchased from the Goodfellow Co., Cambridge, England. The initial procedures of specimen preparation are the same. All specimens, except for the microstructural observations, were prepared as follows. Samples with the size of 10 × 3 × 0.25 mm were cut from the sheet and polished using 800-, 1200-, 1500-, and 4000-grid carbimet papers, then were annealed in a vacuum of 10^{-3} Torr for 4 h at 80 °C, and immediately furnace cooled to the ambient temperature, around 23 °C. Final polishing with 1, 0.5, and 0.05 μm alumina slurries was followed. The thickness for further experimental works is about 0.23 mm, which is less than one-tenth of other dimensions. Specimens of 10 × 10 × 0.25 mm for the SAXS study were prepared in a similar way. Afterward, they were annealed again in a vacuum of 10^{-3} Torr for 4 h at 70 °C and then furnace-cooled to the ambient temperature. This was performed in an EYELA VOS-200SD vacuum-dry oven to remove the residual stress caused by the sample-preparation. All the treated samples were dried in a vacuum desiccator for 3 days at room temperature to eliminate the remaining solvent.

Absorption Measurement. Each absorption sample was preheated in the vacuum for 15 min and then put in a glass test tube filled with acetone at 50 °C. The same procedures as in ref 16 were followed. To monitor the evolution process of crystallization and mass transport, a lot of specimens were

† Department of Materials Engineering.
‡ Department of Physics.
* To whom correspondence should be addressed: Tel (04)-285-2801; FAX (04)-285-7017.

10.1021/ma020851m CCC: $22.00
Published on Web 09/28/2002

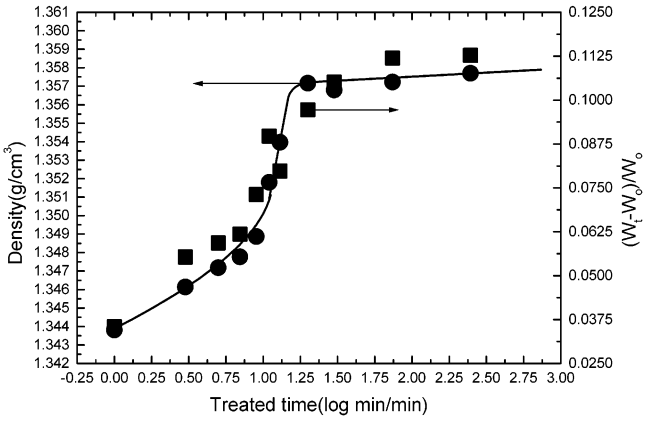

Figure 1. Mass uptake and density vs the solvent-treated time.

prepared with the same procedures and removed during the absorption experiment at different treated times and then kept in a vacuum furnace of 10^{-3} Torr at room temperature for 3 days. The weight gain vs time in logarithmic scale has been plotted in Figure 1, where W_t is the weight of sample at time t and W_0 is the initial mass.

X-ray Measurement. All SAXS measurements were performed at room temperature. The X-ray source with the Cu target is an 18 kW rotating-anode X-ray generator (Rigaku) monochromated by a pyrolytic graphite. One set of three pinhole inherent collimators was used to eliminate the smearing effect inherent in slit-collimated SAXS. The diameters of the first and second pinhole are 1.5 and 1.0 mm, respectively. The size of guard pinhole in front of the sample is 2.0 mm. The scattered intensity was detected by a two-dimensional position sensitive detector (ORDELA Model 2201X, Oak Ridge Detector Laboratory Inc.) with 256 × 256 channels (active area 20 × 20 cm^2 with ∼1 mm resolution). The distance from the sample to detector is 400 cm long. The beam stop is a round lead disk with an 18 mm diameter. All the data were rectified by the background (dark current and empty beam scattering) and the gain response of each pixel of the area detector. The area scattering pattern has been radially averaged to increase the efficiency of data collection as compared to a one-dimensional linear detector. Data were acquired on an IBM-compatible personal computer. The intensity profile was output as a plot of the scattering intensity (I) vs the scattering vector, $q = 4\pi \sin(\theta)/\lambda$ (2θ is the scattering angle).

Density Measurement. The density was measured at 23 °C by a density gradient column filled with a mixture of pure water and concentrated calcium nitrate solution. The detail results are listed in Table 1and were also plotted in Figure 1.

If the densities of amorphous and crystalline phases are assumed to be constants, the weight fraction crystallinity can be derived from[17]

$$W_c(\rho) = [\rho_c(\rho - \rho_a)]/[\rho(\rho_c - \rho_a)] \quad (1)$$

where ρ is the measured density and ρ_c and ρ_a are the densities of a perfect crystal and that of a completely amorphous specimen, respectively. The widely accepted value of ρ_c is 1.455 g cm^{-3}.[18] The general relation between the weight fraction and volume fraction crystallinity, α, is

$$W_c = (\rho_c/\rho)\alpha \quad (2)$$

These results are listed in Table 1 also.

FTIR Spectroscopic Measurement. FTIR measurements were performed in the transmission mode and were carried out in a Bruker EQUINQX55 spectrometer. The example of baseline determinations can be found in our former work.[15] The spectrum of the empty cell was gathered first for the background correction, and the scanning range was from 4000 to 600 cm^{-1}. The resolution is 4 cm^{-1} after computer-averaging a total of 100 scans. The samples were prepared as being soaked in acetone at 50 °C for different periods and then dried in a vacuum desiccator for 3 days. In PET, the band at 973 cm^{-1} can be assigned to the asymmetric C−O stretching mode and is associated with the trans isomer of the −O−C−C−)− group.[19−21] Its intensity is very sensitive to the order state in the polymer.[19,20,22] This peak can be clearly identified through the transmission mode even for a thick sample (ca. 0.25 mm). Therefore, this band was chosen to monitor the change of crystallinity in this study. The conformationally insensitive band at 795 cm^{-1} can be used as an internal thickness standard.[19,23] So the variation of the relative intensity of the absorption band at 973 cm^{-1} can be quantified in terms of the reduced factor, which was obtained from the peak area associated with the 973 cm^{-1} band normalized by that of the 795 cm^{-1} band.[15,19] The way obtaining both peaks by subtraction of the baseline is shown in previous work.[15] Then the area can be calculated through the integration of individual peak. The detail results are listed in Table 1. To compare the results with other works,[24,25] the reduced factor associated with the 898 cm^{-1} band for the gauche isomer was obtained in a similar procedure. The normalized trans content was plotted in Figure 2 together with the results by Koenig et al.[25]

Optical Microscopy Measurement. The transport front can be observed in an Olympus BX60 optical microscope because the material becomes opaque after the solvent resides in PET and the crystallization occurs. The sample following the absorption measurement was cold-mounted using the Struers Speci Fix-20 and left at room temperature for 8 h. Then the sample was sliced by a Struers Minitom and polished to reveal the cross section.

Results and Discussion

When the kinetics is dominated by case I, the sorption is proportional to the square root of time, $t^{1/2}$, whereas the mass uptake is proportional to t for the prevalence of case II. The exponent will be between 0.5 and 1 for the anomalous diffusion.[7,15] The statement above is for the transport process without phase transformation. However, if the solvent-induced crystallization is considered, the introduction of crystalline phase will block the transport and affect the behavior of solvent sorption as discussed later.

Swelling has been suggested as a type of deformation,[15,26] and therefore the variation of sample thickness, 2l, is a convenient indicator of swelling as shown in Figure 3. According to this plot together with the results from OM, it is found that most of swelling occurs as two opposite transport fronts are being merged together. This was consistent with the result of mass uptake as shown in Figure 1. The dramatic increase of mass or solvent concentration before saturation (around treated time 74 min) can be reasonably related to the result of swelling. The Fickian mechanism will not be able to cause such change suddenly since the driving force is the concentration gradient. It seems that diffusional gradients always tend to drive the solvent away from regions of accumulation of solvent unless two transport fronts meet right at the center of the specimen. This accumulation corresponds to an additional pressure that compensates the change of chemical potential of solvent and relaxes as the polymer deforms.[26,27] Therefore, most of the swelling occurs as two fronts meet together in this study.

It is also interesting to see the structural change along with the transport behavior. To investigate the crystallization associated with mass transport, the density, trans conformation, and SAXS vs solvent-treated time were measured in this study. The density basically follows the same trend of mass uptake as shown in Figure 1. Before the sudden rise in density or mass, the

Table 1. Experimental Data of a Combination of SAXS, Density, DSC, and FTIR Spectroscopy for PET under Different Sample Treatments

	treated time (min)										
	1	3	5	7	9	11	13	20	43	74	247
density (g/cm^3)	1.34381	1.34614	1.34718	1.34777	1.34887	1.3518	1.35397	1.35716	1.3568	1.35723	1.3577
crystallinity	0.029	0.051	0.061	0.066	0.077	0.104	0.124	0.154	0.151	0.155	0.159
trans (%)	14.77	17.78	18.25	19.23	20.47	22.11	24.58	27.48	27.63	27.83	28.97

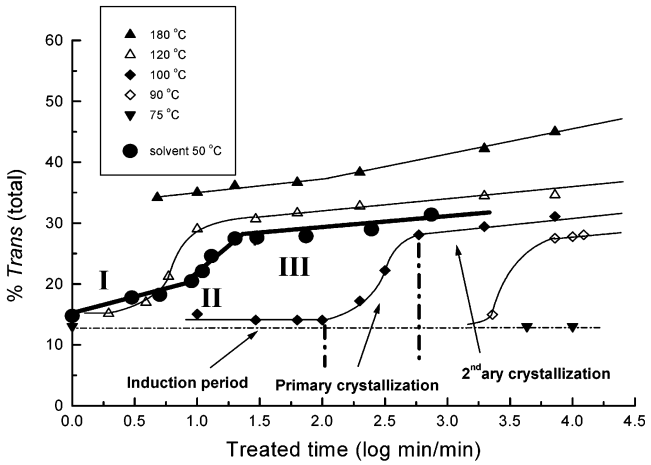

Figure 2. Relative percentage of the trans isomer of PET as a function of treated time for solvent treatment and thermal annealing.

logarithm of mass uptake increases linearly with the logarithm of time with an average slope around 0.32, which implies that the case I mechanism dominates in this region. If the case II mechanism dominated, the coefficient would have been close to 1. This is consistent with the measurement in Figure 3 that the dimensional change is less than 4% before 10 min. The reason that the average slope is below 0.5 is mainly due to the blocking of diffusion by crystallites, and the effect of surface cavitation can be ignored in this system.[1]

The density at the position behind the diffusion front can be expressed as

$$\rho = \alpha\rho_c + (1 - \alpha)\rho_a \tag{3}$$

where α is the volume fraction of crystalline phase and approximately a constant if penetrant transport controlls the extent of induced crystallization in PET and the effect of interface isneglected.[11,28] Here ρ_c and ρ_a are the densities of a perfect crystal and that of a completely amorphous specimen, respectively. The rapid crystallization is consistent with the result that the slope mentioned above is below 0.5 even in the beginning of mass transport, which implies that the transport behavior is affected by the crystallization immediately. Different types of deviation from Fickian behavior in the initial stage have been discussed by Durning et al.[10] From eq 3, the local density difference after crystallization but before the merge of transport front, $\rho - \rho_a$, is equal to $\alpha(\rho_c - \rho_a)$. The average density, ρ_{ave}, at time t is

$$\rho_{ave}(t) = \alpha(\rho_c - \rho_a)d_F(t)/l + \rho_a \tag{4}$$

where d_F is the diffusion distance, and therefore ρ_{ave} possesses the same time dependence as weight uptake before 10 min. This explains why the trends of density and mass variations give similar profiles as presented in Figure 1 in this region. In fact, the penetrant uptake and the sample density were linearly related if the penetrant transport controlled the extent of induced crystallization.[11,29,30] The structural analysis of this crystallization by wide-angle X-ray diffraction has been done in other works.[15,31,32]

After 10 min, the diffusional tails from opposite sides start overlapping. The accumulation of solvent by the case II mechanism can be clearly observed and identified in Figures 1 and 3 since the solvent has no place to be driven away now. The dramatic increase of thickness or swelling at this stage is the feature of the case II mechanism. In fact, the ratio of logarithm of mass uptake to the logarithm of time or the exponent of time is about twice of that in the first stage even for the sample with greater crystallinity in this period. It has been shown that the PET is in a state of compressive strain under the action of the case II mechanism, and the stress relaxed during volume expansion helps to pull out the loops of chains and makes the crystallization proceed much easier.[15] The other important factor for further crystallization to occur is that more depression of glass transition temperature is possible as more solvent transports into the specimen as a result of plasticization.[33] Therefore, a dramatic increase of density in this stage was observed in Figure 1, which suggests a large amount of crystallites formed accompanied by the swelling. At the end of this process, which is around 35 min and close to the saturation of mass uptake, the crystallization rate is slow. This implies that another crystallization process prevails, and it turns out to be the secondary crystallization as discussed later. In fact, Alfrey et al.[2] summarized the mass transport in glassy polymers as follows. If the penetrated concentration is low, swelling is not important so that the transport is controlled by the Fickian law which is often named as case I. On the other hand, if the penetrated concentration is high, swelling is pronounced so that the transport is controlled by stress relaxation. The behavior of mass transport from our measurements basically followed the same trend. In the beginning of mass transport, the concentration of solvent was low, and case I dominated. After that, the concentration increased, and case II prevailed in the second stage. However, the issue about the boundary condition of a fixed constant surface concentration usually used in the model analysis needs to be reconsidered here. To explain the distinct transport behaviors accompanied by dissimilar concentrations inside the specimen at different stages as mentioned above, varied surface concentrations at different periods must be assigned. This is possible here since the phase transformation occurred, and a different metastable state of polymer has been achieved. Therefore, a different chemical potential, which determines the surface concentration, at a different stage is expected. More experimental evidence is being prepared.[28]

The reduced factor at 973 cm^{-1} for the samples acetone-treated for different time can be obtained from the FTIR spectrum as shown in Figure 2 together with

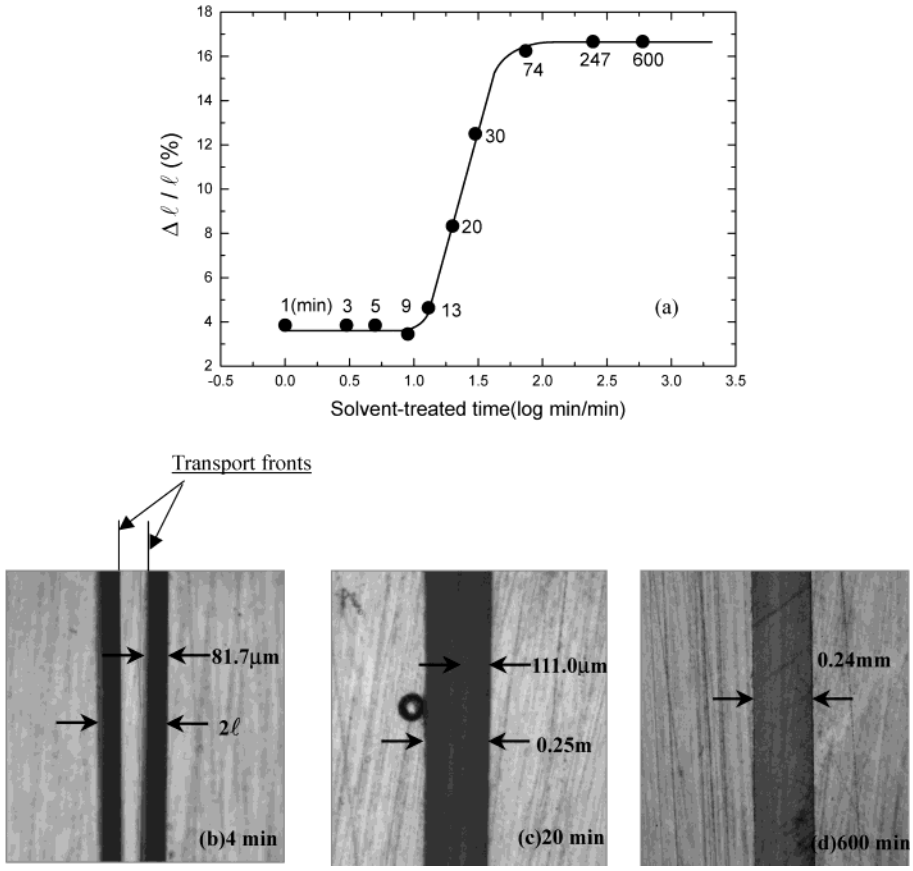

Figure 3. (a) Thickness change vs treated time at 50 °C. (b) Optical micrograph of transport fronts of PET solvent-treated at 4 (c), 20, and (d) 600 min. The black bubble on theleft side of the sample in (c) is related to the matrix of mounting and has nothing to do with the sample.

other results of thermal annealing by Koenig et al.[25] Corresponding three regions as marked in the plot can be found for the solvent-induced crystallization. The reduced factor is roughly linearly proportional to the crystallinity as studied in many works.[19,24] Therefore, the results of the FTIR spectrum about the first two regions are consistent with those mentioned above that a different crystallization process prevails at a different stage. The data of the gauche−trans isomerization in PET by Lin and Koenig[25] have been drawn together with our results. For the low-temperature annealing (less than 160 °C), the two-stage isomerization isotherms, a primary transformation stage followed by a linear secondary process, are distinguished on the logarithmic scale of annealing time. The distinct behaviors below and above 160 °C are due to different mobilities of chain segments, and therefore high and low apparent activation energies are associated with the conducts at low and high temperatures. So the behavior of solvent-induced crystallization can be classified as a low-temperature process. By comparison with the low-temperature annealing conduct, the third stage can be referred to as the "secondary crystallization", and two "primary crystallization" processes are marked as I and II in Figure 2.

The SAXS results can further afford the information on morphology associated with the crystallization process. The q_{max} associated with the local maximum around 0.8 Å^{-1} can be determined from the raw data by fitting a fourth-order polynomial, and the value was found by differentiating the polynomial and setting to zero. The results of q_{max} and its reciprocal are plotted in Figure 4. The reciprocal of q_{max} can be linear

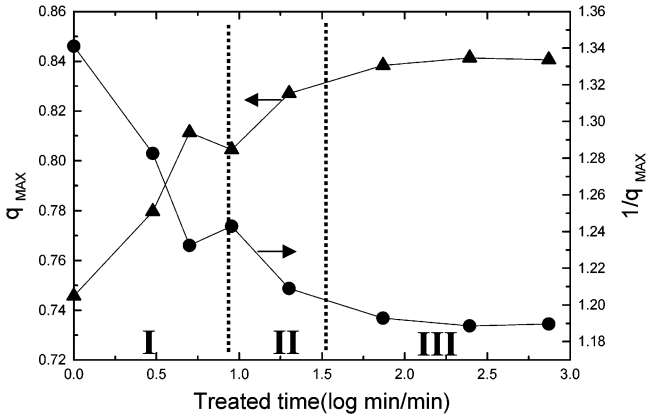

Figure 4. q_{max} (in units of Å^{-1}) and its reciprocal vs the solvent-treated time.

proportional to the long period, L, of lamellae, and decays fast in the region of crystallization dominated by the case I mechanism marked as zone I in the plot. It is well-known that L exhibits a significant decrease during the primary crystallization dominant stage and shows a much slower decrease in the secondary crystallization in PET, which is nearly linear with log time, based on the dual lamellar stack model.[34] Therefore, it is expected to observe two different dramatic decays if the above statements about the three stages of crystallization are correct. This behavior was observed and marked as I and II in Figure 4 for the reciprocal of q_{max}. However, it is interesting to see the rise in the beginning of zone II. This basically suggests that the dual lamellar stack model prevails during the second "primary crystallization" caused by swelling and excludes the pos-

sibility of the lamellar insertion model since the latter predicts the further decrease of L in zone II. Further study of morphological changes during crystallization is being conducted.

Summary

Acetone transport in poly(ethylene terephthalate) and the related crystallization process have been investigated. It is well-known that the effect of surface cavitation can be ignored in this system. Some important results are as follows:

1. Three stages of crystallization were found during the solvent transport in PET from the measurements of density, FTIR, OM, and SAXS.

2. The first stage is caused by the case I mechanism, and the second stage is due to the swelling. The last stage is the secondary crystallization, and most of crystallization occurs during the second stage. The crystallization behavior is strongly affected by the mass transport and vice versa.

3. The results of morphology change during the second "primary crystallization" suggest that the dual lamellar stack model prevails in this period.

Acknowledgment. This work was supported by the National Science Council, Taiwan, Republic of China. The first author dedicates this paper to his father, who passed away while this work was being prepared.

References and Notes

(1) Durning, C. J.; Russel, W. B. *Polymer* **1985**, *26*, 119.
(2) Alfrey, T.; Gurnee, E. F.; Lloyd, W. G. *J. Polym. Sci., Part C* **1966**, *12*, 249.
(3) Wang, T. T.; Kwei, T. K.; Frish, H. L. *J. Polym. Sci., Part A-2* **1969**, *7*, 2019.
(4) Kwei, T. K.; Wang, T. T.; Zupko, H. M. *Macromolecules* **1972**, *5*, 645.
(5) Kwei, T. K.; Zupko, H. M. *J. Polym. Sci., Part A-2* **1969**, *7*, 867.
(6) Wang, T. T.; Kwei, T. K. *Macromolecules* **1973**, *6*, 919.
(7) Perterlin, A. *Makromol. Chem.* **1969**, *124*, 136.
(8) Harmon, J. P.; Lee, S.; Li, J. C. M. *J. Polym. Sci., Part A: Polym. Chem.* **1987**, *25*, 3215.
(9) Harmon, J. P.; Lee, S.; Li, J. C. M. *Polymer* **1988**, *29*, 1221.
(10) Durning, C. J.; Russel, W. B. *Polymer* **1985**, *26*, 131.
(11) Durning, C. J.; Rebenfeld, L.; Russel, W. B.; Weigmann, H. D. *J. Polym. Sci., Part B: Polym. Phys.* **1986**, *24*, 1321.
(12) Durning, C. J.; Rebenfeld, L.; Russel, W. B.; Weigmann, H. D. *J. Polym. Sci., Part B: Polym. Phys.* **1986**, *24*, 1341.
(13) Makarewicz, P. J.; Wilkes, G. L. *J. Polym. Sci., Polym. Phys. Ed.* **1978**, *16*, 1529.
(14) Zachmann, H. G.; Konrad, G. *Makromol. Chem.* **1968**, *118*, 189.
(15) Ouyang, H.; Lee, W.-H.; Shiue, S.-T.; Lin, T.-L. *J. Polym. Sci., Part B: Polym. Phys.* **2002**, *40*, 1444.
(16) Ouyang, H.; Chen, C.-C. *J. Appl. Phys.* **1997**, *81*, 6680.
(17) Alexander, L. E. *X-ray Diffraction Methods in Polymer Science*; Wiley-Interscience: New York, 1969; p 189.
(18) Kitano, Y.; Kinoshita, Y.; Ashida, T. *Polymer* **1995**, *36*, 1947.
(19) Ito, M.; Pereira, J. R. C.; Hsu, S. L.; Porter, R. S. *J. Polym. Sci., Polym. Phys. Ed.* **1983**, *21*, 389.
(20) Miyake, A. *J. Polym. Sci.* **1959**, *38*, 479.
(21) Hannon, M. J.; Koenig, J. L. *J. Polym. Sci., Part A-2* **1969**, *7*, 1085.
(22) Aharoni, S. M.; Sharma, R. K.; Szobota, J. S.; Vernick, D. A. *J. Appl. Polym. Sci.* **1983**, *28*, 2177.
(23) Cunningham, A.; Ward, I. M.; Willis, H. A.; Zichy, V. *Polymer* **1974**, *15*, 749.
(24) Lin, S. B.; Koenig, J. L. *J. Polym. Sci., Polym. Phys. Ed.* **1982**, *20*, 2277.
(25) Lin, S. B.; Koenig, J. L. *J. Polym. Sci., Polym. Phys. Ed.* **1983**, *21*, 2365.
(26) Thomas, N. L.; Windle, A. H. *Polymer* **1982**, *23*, 529.
(27) Silberberg, A. *Macromolecules* **1980**, *13*, 742.
(28) Work in preparation.
(29) Moore, W. R.; Sheldon, R. P. *Polymer* **1962**, *3*, 27.
(30) Cottam, L.; Sheldon, R. P. *Adv. Polym. Sci. Technol.* **1966**, *26*, 65.
(31) Kitano, Y.; Kinoshita, Y.; Ashida, T. *Polymer* **1995**, *36*, 1947.
(32) Sheldon, R. P.; Plakey, P. R. *Nature (London)* **1962**, *195*, 172.
(33) Tashiro, K.; Yoshioka, A. *Macromolecules* **2002**, *35*, 410.
(34) Wang, Z. G.; Hsiao, B. S.; Sauer, B. B.; Kampert, W. G. *Polymer* **1999**, *40*, 4615.

MA020851M